12th International Conference on Fracture Mechanics of Concrete and Concrete Structures
FraMCoS-12
B.L.A. Pichler, Ch. Hellmich, P. Preinstorfer (Eds)

https://doi.org/10.21012/FC12.1216
MS10-2:3

A NOVEL DEM-BASED COUPLED 3D THERMO-HYDRO-MECHANICAL MESOSCOPIC MODEL FOR CRACKED POROUS MATERIALS

M. KRZACZEK[*] AND J. TEJCHMAN[†]

[*] Gdansk University of Technology, Institute of Mechanics of Materials and Structures
Narutowicza 11/12, 80-233 Gdańsk, Poland
e-mail:marek.krzaczek@pg.edu.pl, www.pg.edu.pl

[†] Gdansk University of Technology, Institute of Mechanics of Materials and Structures
Narutowicza 11/12, 80-233 Gdańsk, Poland
e-mail:jacek.tejchman@pg.edu.pl, www.pg.edu.pl

Key words: DEM/CFD, Porous Materials, Heat Transfer, Thermo-Hydro-Mechanical model

Abstract: Most of the physical phenomena in engineering problems occur under non-isothermal conditions. The occurrence of some physical phenomena or chemical reactions can lead to local temperature changes and, consequently, to heat transfer and even local phase changes in the fluid. The need to consider the effect of heat transfer and phase changes in the fluid becomes critical in analyses of many multi-field problems in porous and fractured materials. A novel DEM-based pore-scale 3D thermo-hydro-mechanical (THM) model of two-phase fluid flow and heat transfer in fluid and solids is based on a direct numerical simulation approach. The model's original concept is based on the notion that in a physical system, two domains coexist: the 3D discrete (solid) domain and the 3D continuous (fluid) domain. Both domains are discretized into a coarse mesh of tetrahedra. The THM model was validated by comparing the numerical results with the analytical solution of the classic 1D heat transfer problem. Numerical calculations were carried out for bonded granular specimens imitating concrete with a 3D DEM fully coupled with 3D CFD (based on a fluid flow network) and 3D heat transfer that linked discrete mechanics with fluid mechanics and heat transfer at the meso-scale. The heat transfer was related to the fluid (diffusion and advection) and bonded particles (conduction). Bonded particle assemblies with random grain distribution were considered. Perfect accordance was obtained between numerical and analytical outcomes. In addition, the effects of a macro-crack in the specimen on the distribution of fluid pressure, density, velocity, and temperature were studied.

1 INTRODUCTION

The majority of physical phenomena in engineering challenges happen in non-isothermal environments. Furthermore, even if the physical system is initially in thermodynamic equilibrium, physical processes or chemical reactions may cause local temperature differences, resulting in heat transfer. In analyzing many multi-field issues in porous of many multi-field issues in porous and fractured materials, the requirement to address the effect of heat transport becomes crucial. Diffusion, advection, and radiation are the basic heat transfer phenomena. These phenomena influence the mechanical response of the system.

The most popular technique applied in thermo-hydro-mechanical (THM) models is a continuum one. The continuum model is based on a mathematical framework linking sets of differential equations to explain thermodynamic, solid, and fluid mechanics laws, such as finite element [1]-[3], or finite difference implementations [4]. Even though they are appealing for macro-scale applications, continuum modeling approaches based on the finite element method (FEM) or the finite volume method (FVM) have

significant computational and continuity limitations when applied to discontinuous and highly deformable media like packed or fluidized beds and fractured granular porous materials. Classical approaches have tremendous numerical challenges generating suitably fine meshes in porous media with low porosity (less than 15%), such as concrete or rocks [5]. Discrete techniques, such as the discrete element method (DEM) [6] or the finite-discrete element method (FDEM) [7], [8], on the other hand, proved to be successful in modeling the behavior of particulate systems. The capacity to directly predict fracture evolution through particulate materials is a benefit of DEM.

Various methods were adopted to combine DEM with fluid flow and heat transfer phenomena. To connect TH processes with DEM, direct numerical simulations (DNS) could be used. Different numerical approaches (for example, FEM and FVM) were applied to solve governing equations. Deen et al. [9] suggested a method for implementing submerged boundaries that did not require the use of an effective diameter. THM processes in dense fluid-particle systems were the subject of the approach. The proposed approach was confined to invariant geometries, topologies, and porosities of relatively high values (porosities greater than those of concrete or rock). DNS-DEM models, in reality, are limited to systems with fewer particles than CFD models. The lattice Boltzmann methods (LBMs) [10], [11], [12] rely heavily on the precise depiction of solid-fluid interfaces and have the same numerical and computational restrictions as DNS-DEM models. Recently, most DEM-based THM models separated fluid flow within reservoirs (pores, pre-existing cracks, etc.) from the flow between reservoirs [13], [14]–[17].

The purpose of this work is to demonstrate a novel DEM-based pore-scale hydro-mechanical model of two-phase fluid flow and heat transfer in partly saturated porous materials with very low porosity like concrete subjected to fracture. THM calculations were carried out using a 3D DEM in conjunction with 3D CFD (based on a fluid flow network made up of channels) and 3D heat transfer, which connected discrete mechanics, fluid mechanics, and heat transfer at the meso-scale. Previously, a coupled 2D DEM/CFD model based on the fluid flow network without heat transfer (formulated by the authors [18], [19]) was used to describe hydraulic fracturing in partly saturated rock masses with one- or two-phase laminar viscous two-phase fluid flow containing a liquid and gas.

This paper's DEM-based THM mesoscopic technique for modeling fluid flow and heat transfer has substantial advantages over other existing ones in the literature. Some of the advantages are as follows:

1. the precise tracking of water/gas fractions in pores, taking into account their variable geometry, size, and position,
2. a novel method for automatic local meshing and re-meshing particle and fluid domains to account for changes in their geometry and topology,
3. the use of a coarse mesh of solid and liquid domains to generate a virtual fluid flow network (VPN) and to solve the energy conservation equation,
4. using FVM to solve the energy conservation equation in both domains on a very coarse mesh of cells,
5. to examine supercritical fluid flow, the corrected Peng-Robinson equation of state [20] was adopted for both fluid phases (necessary e.g. for studying THM processes in hydraulic fracturing problems),
6. tracking virtual thermal deformation of discrete elements to precisely compute fluid volume changes over time, and
8. two-phase flow.

The structure of the current study is outlined below. Following Section 1, a mathematical model of the DEM-based linked thermal-hydro-mechanical method is provided in Section 2. The validation of the THM model is described in Section 3. The influence of advection on the cooling of a bonded granular assembly is examined in Section 4. A damage process in a bonded granular assembly during a thermal contraction test is discussed in Section 5. Finally, in Section 6, some closing remarks are made.

2 THM MODEL

The THM model's original concept is based on the notion that in a physical system, two domains coexist: the 3D discrete (solid) domain and the 3D continuous (fluid) domain (Fig.1a). Next, both domains are treated as continuous and are discretize (Fig.1b). As a result, discrete element equations of motion are solved in the 3D discrete domain, whereas fluid flow and heat transfer equations are solved in the 3D continuous domain (red color in Fig.1 and Fig.1b).

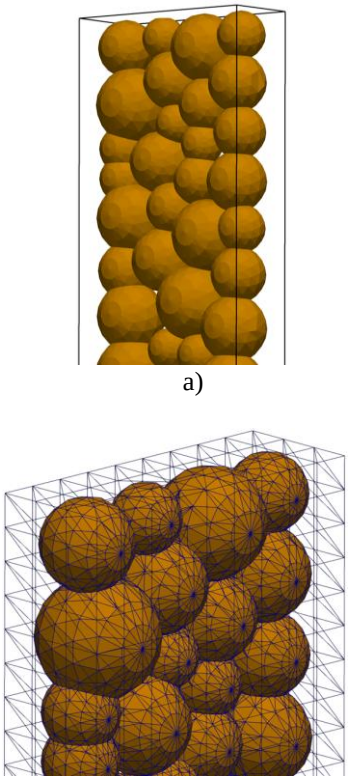

a)

b)

Figure 1: Two domains coexisting in one physical system: a) before discretization and b) solid and fluid domain after discretization.

2.1 DEM for cohesive-frictional materials

DEM calculations were performed with the 3D spherical explicit discrete element open code YADE [21], [22] that allows for a small overlap between two contacted bodies (soft-particle model). Utilizing an explicit time-stepping scheme, particles in DEM interact with one another during translational and rotational motions using a contact law and Newton's 2nd law of motion [6]. A cohesive bond at the grain contact is postulated in the model, with brittle failure beneath the critical normal tensile force. Under normal compression, shear cohesion failure causes contact slip, which follows the Coulomb friction law. Non-viscous damping was applied [23] to accelerate convergence in quasi-static simulations.

The following material constants: E_c, υ_c, μ_c, C (cohesive contact stress), and T (tensile normal contact stress) are required for DEM simulations. In addition, R (particle radius), ρ, (mass density), and α_d (positive damping coefficient smaller than 1) are needed. The C/T ratio is crucial to adequately simulate the failure type of specimens (brittle or quasi-brittle), the distribution of shear and tensile cracks, and the ratio between the uniaxial compressive and tensile strength. The material constants are usually identified by running a series of DEM simulations and comparing them with experimental results of simple tests (e.g. uniaxial compression, triaxial compression, simple shear) [24]. The damping parameter is always α_d=0.08. For this value, the loading velocity v does not affect the results [24]. Damage occurs if a cohesive joint between spheres disappears after reaching a critical threshold. If any contact between spheres after failure re-appears, the cohesion does not appear more. Note that material softening is not considered in the DEM model. Although bonds can break by shear, the essential micro-scale mechanism for damage in the pre-failure regime is bond damage in tension. An arbitrary micro-porosity might be achieved in DEM since the particles may overlap. The fracture is not allowed to propagate through aggregate, i.e. the particle breakage is not taken into account. The model was successfully used by the authors for describing the behavior of different engineering materials with a granular structure (mainly of granular materials [25]-[28]) and concrete materials [29]-[34] by taking shear localization and fracture into account).

2.2 Fluid flow model

The general concept of a fluid flow algorithm using DEM and a channel network is adopted from [13]-[14]. In this concept, fluid flow is simulated by assuming that each particle contact is an artificial flow channel (between two parallel plates in 2D or along a duct in 3D) and those artificial channels connect real reservoirs in the particulate medium (pores, fractures, and pre-existing cracks) that store fluid pressures. Thus, the pressure in reservoirs depends both on the mass transported along channels from/to other reservoirs and the volume changes of reservoirs. Since the volume of reservoirs changes due to the material deformation (described by discrete elements in DEM), the fluid density must also change (the fluid in reservoirs is compressible). Thus, the fluid moves in channels while the reservoirs solely store pressure. The artificial channels create a fluid flow network. The fluid flow in those artificial channels is characterized by a simplified laminar flow of an incompressible fluid as

opposed to the compressible fluid model in real reservoirs. The fluid model in the current paper significantly differs from the general concept [13]-[14]. The reservoirs (pores, cracks, pre-existing cracks, etc.) store now not only pressures but also phase fractions, fluids densities, energy, and temperature. The continuity equation is employed to compute the density of fluid phases stored in reservoirs. The fluid phase fractions in reservoirs are computed by applying the equation of state for each phase assuming that fluid phases share the same pressure (as in the Euler model of multi-phase flow). The mass flow rate in artificial channels of a fluid flow network is now estimated by solving continuity and momentum equations for the laminar flow of incompressible fluid. The 3D spherical particles are discretized into the 3D tetrahedrons [18]. To get a more realistic distribution of the unknown variables (pressure, fluid-phase fractions, and densities), a re-meshing procedure discretizes the overlapping spheres, determines the contact surfaces, and deletes the overlapping areas [18]. As a result, each reservoir is discretized into several tetrahedrons (in 3D problems). Each tetrahedron in the fluid domain is called the Virtual Pore (VP). The artificial channels connect the gravity centers of tetrahedrons (VPs) to create a fluid flow network called the Virtual Pore Network (VPN). All forces converted from pressure and shear stress are applied to the spheres. All numerical parameters might be used without the necessity of re-calibration. VPs accumulate pressure and store both fluid-phase fractions and densities, energy, and temperature. The mass change in VPs is related to the density change in a fluid phase that results in pressure variations. The equation of momentum conservation is neglected in tetrahedrons but the mass is still conserved in the entire volume of tetrahedrons.

The numerical algorithm can be divided into 5 main stages:

a) estimating the mass flow rate for each phase of fluid flowing through the cell faces (in channels surrounding VP) by employing continuity and momentum equations,
b) computing the phase fractions and their densities in VP by employing equations of state and continuity,
c) computing pressure in VP by employing the equation of state,
d) solving the energy conservation equation in fluid and solids,
e) updating material properties.

This algorithm is repeated for each VP in VPN and each solid cell (stage ‘d’) using an explicit formulation. According to the above algorithm, incompressible laminar two-phase fluid (liquid/gas) flow under non-isothermal conditions is assumed in the channels of the fluid flow network. The liquid and gas initially exist in the material matrix and pre-existing discontinuities. The channel length is assumed to be equal to the distance between the gravity centers of adjacent grid tetrahedrons.

The hydraulic aperture of the channel is directly related to the geometry of the adjacent tetrahedrons as

$$h = \gamma e \cos(90^{\circ} - \omega) \tag{2}$$

where e is the edge length between two adjacent tetrahedrons, ω denotes the angle between the edge with the length e and the centerline of the channel that connects two adjacent tetrahedrons and γ is the reduction factor, necessary to fit the fluid flow intensity to actual complex fluid flow conditions in materials. The reduction factor γ is determined in parametric studies to keep the maximum Reynolds number R_e along the main flow path always lower than the critical one for laminar flow.

2.2 Mass flow rate in channels

Three flow regimes in the VPN channels are distinguished: a) single gas-phase flow with gas-phase fraction α_p=1, b) single liquid-phase flow with liquid phase fraction α_q=1 and c) two-phase flow (liquid and gas) with $0<\alpha_q<1$. For single-phase flow in channels (flow regime ‘a’ and ‘b’), the fluid moves in channels through a thin film region separated by two closely spaced parallel plates according to a classical lubrication theory [35], based on the Poiseuille flow law [36]. As a result, the mass flow rate of the single-phase flow along channels is

$$M_x = \rho \frac{h^3}{12\mu} \frac{P_i - P_j}{L} \tag{1}$$

where M_x - the mass fluid flow rate (per unit length) across the film thickness in the x-direction [kg/(m s)], h - the hydraulic channel aperture (its perpendicular width) [m], ρ - the fluid density [kg/m^3], t - the time [s], μ - the dynamic fluid (liquid or gas) viscosity [Pa s] and P - the fluid pressure [Pa] (P_i and P_j are the pressures in the adjacent VPs).

A two-phase flow of two immiscible and incompressible fluids in a channel is assumed to simulate a two-phase fluid flow (flow regime 'c'), driven by a pressure gradient in adjacent VPs. The liquid-gas interface is parallel to the channel plates and constant along the channel. Gravity forces are neglected. The interface between the fluids, labeled as *j*=*q*, *p* (*q* - the lower liquid phase and *p* – the upper gas phase), is assumed to be flat in the undisturbed flow state. Under this assumption, the model allows for a plane-parallel solution. The interface position is known and is related to fractions of fluid phases in adjacent VPs while the volumetric flow rates of fluid phases are unknown.

Continuity and momentum equations characterize the flow in each phase. The time and pressure are scaled by h_p/u_i and $\rho_p u_i^2$ (h_p - the height of the upper layer and $\mathbf{u}_i$ - the interfacial velocity). The dimensionless continuity and momentum equations are presented in [37].

The solution details are presented in [19]. Solving equations with boundary conditions, the mass flow rates $M_{q,x}$ and $M_{p,x}$ for both fluid phases are calculated as well as the shear stress τ_{f0} at the channel surfaces.

2.2.2 Fluid flow in virtual pores

VPs, in contrast to the channel flow model, assume that the fluid is compressible. The fluid pressure can reach 70 MPa in specific situations, such as during the hydraulic fracturing process. The gas phase exceeds the critical point and becomes a supercritical fluid under these conditions. For both fluid phases in VPs, the Peng-Robinson equation of state [20] is used to describe fluid behavior above the critical point.

For most substances, the Peng-Robinson equation of state provides a good fit for the vapor pressure, however predicting molar volumes can be very inaccurate. The forecast of saturated liquid molar quantities might deviate by l0-40% [38]. Peneloux and Rauzy [39] proposed an effective correction term

$$V_a^{corr} = V_a + s, \tag{2}$$

where s is the small molar volume correction term that is component dependent; V_q is the molar volume predicted by Eq.2 and V_q^{corr} refers to the corrected molar volume. The value of *s* is negative for higher molecular weight non-polar and essentially for all polar substances.

For each phase, the mass conservation equation is used. The mass transfer between phases and the grid velocity is till now ignored when there is no internal mass source. The discretized form of the mass conservation equation for the liquid phase is

$$\frac{\alpha_{q,i}^{n+1}\rho_{q,i}^{n+1}V_i^{n+1} - \alpha_{q,i}^{n}\rho_{q,i}^{n}|}{\Delta t} + \sum_f \left(\rho_{q,f}^n U_f^n \alpha_{q,f}^n\right) = 0$$

$$V_i^{n+1} = V_i^n + \frac{dV}{dt}\Delta t \tag{3}$$

where *f* is the face (edge) number, U_f^n denotes the volume flux through the face [m^3/s], based on the average velocity in the channel, $\alpha_{q,f}^n$ is the face value of the fluid phase volume fraction [-], *t* is the time step [s], *n* denotes the time increment and *i* is the VP number [-]. The explicit formulation is used instead of an iterative solution of the transport equation during each time step since the volume fraction at the current time step is directly computed from known quantities at the previous time step. Similarly, the mass conservation equation for a gas phase is introduced. The product $\rho_q U_f^n \alpha_{q,f}^n$ in Eq.3 is the mass flow rate $M_{q,f}$ of the liquid phase flowing through the face *f* of VP$_i$. The density of the liquid phase can be calculated by solving the mass conservation equation for both phases.

Because the fluid phases share the same pressure the liquid phase fraction is computed. The gas-phase fraction is computed as $\alpha_{p,i}^{n+1} = 1 - \alpha_{q,i}^{n+1}$. Equation of state is used to calculate the new pressure P_i^{n+1} in VP$_i$.

2.3 Heat transfer

Heat is transferred in both the fluid and solid domains. When it comes to heat transfer in multi-phase fluid flow, the temperature is shared, but enthalpy is transferred. The heat transfer model is simplified. A homogeneous heat transfer model is assumed in multiphase flow (mass transfer between phases is not supposed to be taken into account). The multiphase fluid is homogenized to a single-phase fluid. The effective fluid properties and velocity are calculated using volume averaging over the phases. The numerical solution uses

the same very coarse mesh of both domains (Fig.1b) that is used to create the fluid flow network to solve the governing equations.

2.3.1 Heat transfer in fluid

The fluid is incompressible and homogeneous. The viscous dissipation of energy is not taken into account. The energy conservation equation is shared by all phases in the homogeneous model and is expressed in integral form

$$\int_V \frac{\partial \rho_{eff} E}{\partial t} dV + \oint \rho_{eff} \vec{v} E \cdot d\vec{A} = \oint \lambda_{eff} \nabla T \cdot d\vec{A} + \int_V S_h, \quad (4)$$

where ρ_{eff} is the effective density of the fluid [kg/m^3], E denotes the total energy [J], t is the time [s], $\vec{v}$ is velocity vector [m/s], T is the temperature [K], λ_{eff} denotes the effective thermal fluid conductivity [W/(mK)] and S_h represents the energy source term. Assuming an incompressible and laminar flow of the homogeneous fluid, the enthalpy h equation of state is

$$h = \int_{T_{ref}}^{T} c_p dT, \quad (5)$$

where T_{ref} is the reference temperature [K] and c_p denotes the specific heat for constant pressure [J/(kg·K)]. The effective fluid properties and velocity are computed by volume averaging over the phases. The specific heat capacity is assumed to be independent of composition and pressure.

$$c_p = \sum_i \alpha_i c_{pi} = const. \quad (5)$$

Equation 4 is applied to each fluid cell (tetrahedron) in the computational domain. The finite volume method is used to solve Eq.4.

2.3.2 Heat transfer in solid

The energy conservation equation has the following integral form if there is no internal heat sources, and constant density in solid regions

$$\rho_s \int_V \frac{\partial E}{\partial t} \cdot dV = \oint (\lambda_s \nabla T) \cdot d\vec{A}, \quad (6)$$

where E is the total energy, equal to enthalpy $h = \int_{T_{ref}}^{T} c_p dT$, ρ_s denotes the solid density [kg/m^3], λ_s is the thermal conductivity of solid [W/(mK)], T_{ref} denotes the reference temperature and c_p is the specific heat in constant pressure. Equation 6 is applied to each cell (tetrahedron) in the solid domain. The total energy is calculated using the enthalpy equation of the state

$$E = c_p(T - T_{ref}). \quad (7)$$

The DEM-based THM model was implemented by the authors into the open-source software package YADE [22] which is already parallelized by computer cluster nodes using the OpenMPI library.

3 VALIDATION OF THM MODEL

The THM model was validated by comparing the numerical findings with the analytical solution for the classic 1D heat transfer problem (diffusion) in the cohesive granular bar specimen

$$\frac{\partial T}{\partial t} = \alpha_{eqv} \frac{\partial^2 T}{\partial x^2}, \quad (8)$$

where α_{eqv} is the effective thermal diffusivity [m^2/s] and t is the time [s]. The initial and boundary conditions for the analytical solution of the 1D heat equation are as follows

$$T(x,0) = 323.16 \ \text{[K]} \quad x \in <0, L>, \quad (9)$$

$$T(0,t) = T(L,t) = 293.16 \ \text{[K]} \quad t \geq 0, \quad (10)$$

where L is the length of the bar. Using the Fourier series, the unsteady solution becomes

$$T(x,t) = \sum_{n=1}^{\infty} D_n \sin\frac{n\pi x}{L} e^{\alpha \frac{n^2 \pi^2 t}{L^2}}, \quad (11)$$

where

$$D_n = \frac{2}{L} \int_0^L T(x,0) \sin\frac{n\pi x}{L} dx. \quad (12)$$

The calculations were performed using a bonded granular bar specimen with a random

distribution of spheres (Fig.2a). The effective thermal diffusivity α_{eqv} was calculated for the volume-averaged phase properties

$$\alpha_{eqv} = \frac{\lambda_{eff}}{c_{p,eff}\rho_{eff}}, \tag{13}$$

where

$$\lambda_{eff} = \frac{1}{V_r}\sum_k \lambda_k V_k ,$$
$$c_{p,eff} = \frac{1}{V_r}\sum_k c_{p,k} V_k \tag{14}$$
$$\rho_{eff} = \frac{1}{V_r}\sum_k \rho_k V_k$$

and V_r - the total volume of the bar specimen [m^3], k - the phase index, V_k - the k-phase volume [m^3], λ_k - the heat conductivity of the phase k [W/(m·K)], $c_{p,k}$ is the specific heat in constant pressure of the phase k [J/(kg·K)] and ρ_k is the phase density k [kg/m^3]. The initial and boundary conditions are shown in Fig.2b (the bar specimen was cooled down by 30 K). The effective thermal diffusivity and boundary conditions imitated heat transfer by diffusion only in the equivalent solid bar, made of a fictitious homogeneous material with effective thermal properties (Eq.14). The single-phase flow of water was assumed.

The numerical results of cooling the concrete bar specimen with a random distribution of spheres (Fig.2a) were compared to an analytical solution of the one-dimensional diffusion problem in an equivalent solid bar. In general, all properties of a fluid flowing under non-isothermal conditions are more or less temperature-dependent. The most important property of a fluid is density. The DEM-based THM model uses the corrected Peng-Robinson equation of state to calculate the fluid phase density. Hence, the density depends on temperature and pressure. In this study, it was assumed for the sake of simplicity that other fluid properties were independent of temperature since most of the simulations presented were performed for a maximum temperature difference of 30 K. In that temperature range, the dynamic viscosity of the fluid slightly changed only. Therefore, we neglected the temperature dependence of viscosity in the current paper and the thermal properties of the fluid.

From the phase properties, the effective material properties of the equivalent solid were determined using Eq.14: $\lambda_{eff} = 3.357\,\frac{\mathrm{W}}{\mathrm{m\cdot K}}$, $c_{p,eff} = 929.51\,\frac{\mathrm{J}}{\mathrm{kg\cdot K}}$ and $\rho_{eff} = 2422.74\,\frac{\mathrm{kg}}{\mathrm{m^3}}$. For a time value of 100 s, the comparison results in Fig.3 are shown.

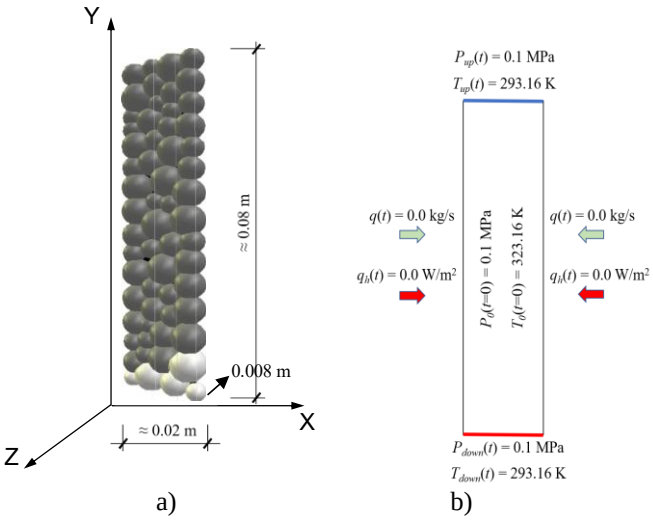

Figure 2: Bonded bar specimen during diffusion simulations: a) bar specimen and b) initial and boundary conditions (q - fluid mass flow rate and q_h - heat transfer rate)

The numerical results agree with the analytical solution. After 100 s of cooling, the largest difference between numerical and analytical values was 0.98 K. The density ranged from 1000.02 kg/m^3 to 1014.28 kg/m^3 after 100 s of cooling. In the estimation of the water density, the Peng-Robinson equation of state with a correction generated little inaccuracy (less than 1.3%). The fluid density was slightly overestimated. For single-phase fluids and flow regimes near stagnant flows, the Peng-Robinson equation of state offers no significant advantages over other models (e.g. IAPWS for water and steam).

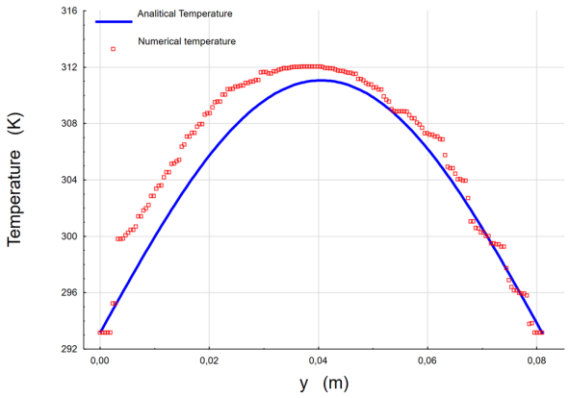

Figure 3: Temperature along vertical center line of cohesive granular bar specimen during cooling after t=100 s

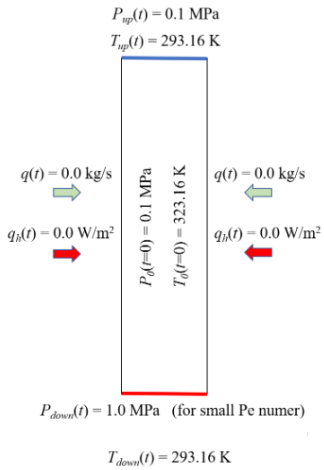

Figure 4: Initial and boundary conditions in cohesive granular bar specimen during diffusion and advection (q - fluid mass flow rate and q_h - heat transfer rate)

3 EFFECT OF ADVECTION ON COOLING OF BAR SPECIMEN

A random distribution of spheres (Fig.2a) was used to evaluate the effect of advection on the cooling of the bonded bar specimen (imitating concrete). One simulation type was carried out: for a low Peclet (Pe) number. The assumption was that water flowed in a single phase. Heat transfer in the bar specimen was simulated by diffusion (due to temperature differences) and advection (due to fluid mass movement) using the initial and boundary conditions in Fig.4. The bar specimen was cooled down again by 30 K. The one pressure difference between the two edges of the bar specimen was defined: 0.9 MPa (low Peclet number). The numerical results are demonstrated in Figs.5-6.

After t=100 s of cooling, the temperature difference between diffusion without advection and diffusion with advection reached 1.09 K (Fig.5). The maximum Peclet number in the fluid domain was 24.

The advection accelerated a cooling process. The fluid velocity was very small; it did not exceed a velocity of $8.92 \cdot 10^{-9}$ m/s. The velocity vectors were almost parallel to the vertical sides (Fig.6), indicating that the fluid flow in the bar specimen was 1D. From the bottom to the top, the fluid pressure varied approximately linearly along the bar specimen. After 100 s of cooling, the fluid density ranged from 995.7 to 1012.5 kg/m^3. In the density estimation, the Peng-Robinson equation of state with a correction produced an insignificant error (less than 1.3%) (the fluid density was slightly overestimated).

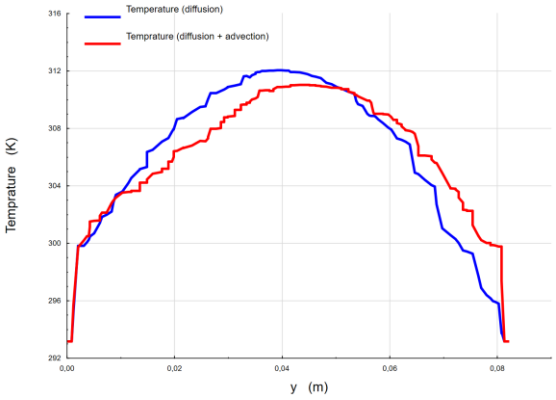

Figure 5: Temperature along vertical center line of cohesive granular bar specimen during cooling after t=100 s (diffusion in blue color, and diffusion + advection in red color)

In comparison to diffusion-only heat transfer, the temperature change along the vertical centerline was not symmetric. As a result of a colder fluid flowing (advection) in the same direction as the temperature shift, a significant spatial shift of the temperature happened in the fluid flow direction (Fig.6). The temperature of the bar fluctuated very little along its horizontal cross-section. The largest temperature difference in the bar's middle horizontal cross-section was only 0.008 K.

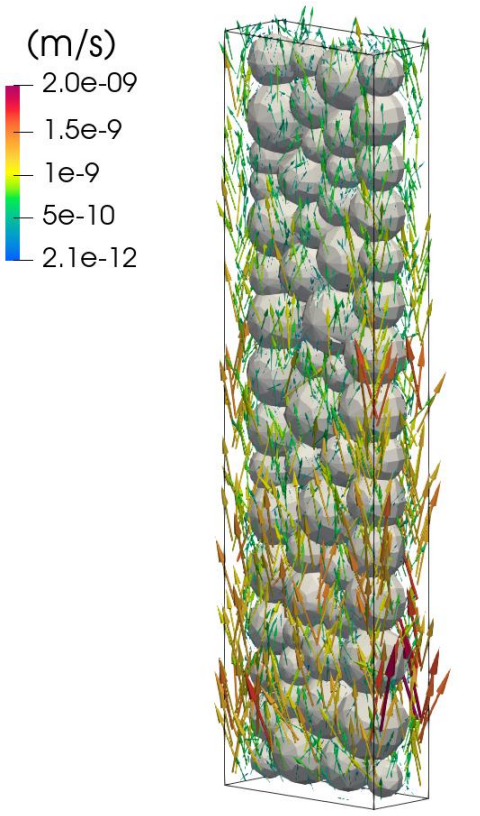

Figure 6: Fluid velocity vectors in bonded bar specimen after cooling time of *t*=100 s due to diffusion and advection

4 THERMAL CONTRACTION TEST

A thermal contraction test during cooling of the bonded bar specimen with a random distribution of spheres was performed (Fig.2a). To eliminate advection at the start of the cooling process and keep the fluid beyond the phase change conditions, the boundary and initial conditions of Fig.7 were used. The flow of two-phase fluids was studied. The bar specimen was composed of 80% water and 20% air. Sphere displacements and rotations were fixed at both ends of the specimen.

To accelerate the heat transfer process and its effect on the damage mechanism in the specimen, the water and air heat transfer coefficients were multiplied by 10, and the solid heat transfer coefficient of 420 W/(m K) (typical for silver) was adopted. Solids were assumed to have a thermal (linear) expansion coefficient of 0.00083 1/K.

Figure 8 illustrates a deformed bar specimen with a macro-crack, broken normal sphere contacts, and sphere displacements after 17 s of cooling.

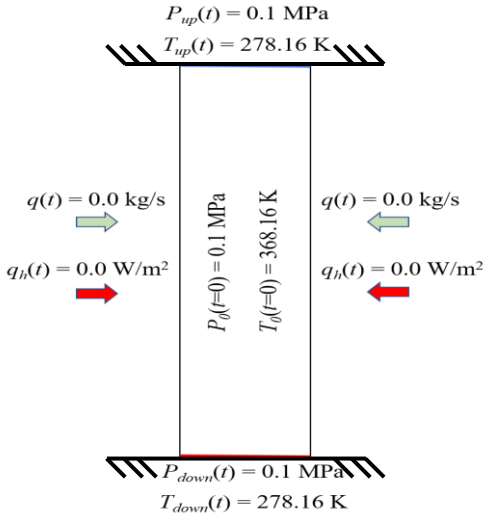

Figure 7: Initial and boundary conditions in cohesive granular bar specimen in thermal contraction test (q - fluid mass flow rate and qh - heat transfer rate)

Figure 8: Grain diameter reduction in bonded bar specimen during thermal contraction test after time t=17 s (largest diameter reduction is in black, smallest diameter reduction is in white)

The temperature distribution in the bar specimen in thermal contraction test in entire specimen and along vertical center line is shown in Fig.9.

The temperature was the highest (333.44 K) in the specimen near the macro-crack edge (Fig.9a). A macro-crack occurred in the bar specimen due to tension. It was created at the bar specimen's weakest zone near the top edge in a slightly different location than during pure uniaxial tension. There was a noticeable vertical movement of spheres in the specimen mid-region. The mean diameter of spheres d_{50} reduced from 6.032 mm to 5.837 mm (by

around 3%) with the smallest changes in the bar's mid-region.

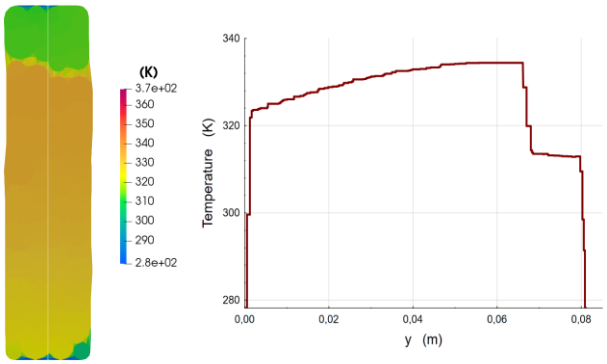

Figure 9: Temperature distribution in bonded bar specimen in thermal contraction test after time t=17 s: a) in vertical mid-cross-section of specimen and b) along vertical center line

In the damaged location, the fluid pressure dropped to 0.0116 MPa (0.0884 MPa below the original pressure). Once the normal contacts broke and the macro-crack began to expand, the pressure drop was produced by an increase in fluid volume in the damaged area due to tensile strain.

5 CONCLUSIONS

This work proposes a new DEM-based pore-scale thermal-hydro-mechanical model of two-phase fluid flow in partially saturated porous materials with low porosity (like concrete) that was coupled with heat transfer. The numerical findings were compared to the analytical solution of the 1D heat transfer problem in an analogous bonded bar specimen to validate the model. The effect of advection was also investigated. Based on mesoscale simulations, the following conclusions can be offered:

During the 1D heat transfer problem, the largest temperature difference between numerical and analytical findings was just 0.98 K.

Advection increased the cooling of the specimen. The highest temperature difference between cooling by diffusion and cooling by diffusion with advection was 1.09 K after 100 s of cooling with a pressure decrease of 0.9 MPa at the specimen height.

The pressure difference between the two edges of the specimen increased the Peclet number to 24 and caused a significant right shift of the temperature distribution along the vertical centreline of the specimen.

REFERENCES

[1] Olivella S., Gens A., Carrera J., Alonso E., Numerical formulation for a simulator (code bright) for the coupled analysis of saline media. *Eng. Comput*. 13 (7) (1996) 87–112.

[2] Kolditz O., Bauer S., Bilke L., Böttcher N., Delfs J.O., Fischer T., Görke U.J., Kalbacher T., Kosakowski G., McDermott C.I., Park C.H., Radu F., Rink K., Shao H., Shao H.B., Sun F., Sun Y.Y., Singh A.K., Taron J., Walther M., Wang W., Watanabe N., Wu Y., Xie M., Xu W., Zehner B., Opengeosys: an open-source initiative for numerical simulation of thermo-hydro-mechanical/chemical (thm/c) processes in porous media. *Environ. Earth Sci.* 67 (2) (2012) 589–599.

[3] Zareidarmiyan A., Salarirad H., Vilarrasa V., Kim K.-I., Lee J., Min K.-B. Comparison of numerical codes for coupled thermo-hydro-mechanical simulations of fractured media. *Journal of Rock Mechanics and Geotechnical Engineering* 12 (2020) 850-865.

[4] Rutqvist J., Wu Y.-S., Tsang C.-F., Bodvarsson G. A modeling approach for analysis of coupled multiphase fluid flow, heat transfer, and deformation in fractured porous rock. *Int. J. Rock Mech. Min. Sci.* 39 (4) (2002) 429–442.

[5] Abdi R., Krzaczek M., Tejchman J. Comparative study of high-pressure fluid flow in densely packed granules using a 3D CFD model in a continuous medium and a simplified 2D DEM-CFD approach. *Granular Matter* 24, 15 (2022), https://doi.org/10.1007/s10035-021-01179-2.

[6] Cundall P., Strack O., A discrete numerical model for granular assemblies. *Géotechnique* 29 (1) (1979) 47–65.

[7] Yan C., Zheng H.. A coupled thermo-mechanical model based on the combined finite-discrete element method for simulating thermal cracking of rock. International Journal of Rock Mechanics & Mining Sciences 91 (2017) 170–178.

[8] Yan C., Xie X., Ren Y., Ke W., Wang G. A FDEM-based 2D coupled thermal-hydro-mechanical model for multiphysical simulation of rock fracturing. I. J. of Rock Mechanics & Mining Sciences 149 (2022) 104964.

[9] Deen N. G., Kriebitzsch S. H., van der Hoef M.A., Kuipers J. Direct numerical simulation of flow and heat transfer in dense fluid–particle systems, *Chem. Eng. Sci*. 81 (2012) 329–344.

[10] Chen Z., Jin X., Wang M. A new thermo-mechanical coupled DEM model with non-spherical grains for thermally induced damage of rocks. *J. Mechanics and Physics of Solids*, 116 (2018) 54-69.

[11] Jiao K., Han D., Li J., Bai B., Gong L., Yu B. A novel LBM-DEM based pore-scale thermal-hydro-mechanical model for the fracture propagation process. *Computers and Geotechnics*, 139 (2021) 104418.

[12] Yang B., Chen S., Liu K. Direct numerical simulations of particle sedimentation with heat transfer using the lattice boltzmann method, *Int. J. Heat Mass Transfer* 104 (2017) 419–437.

[13] Cundall P. Fluid formulation for PFC2D. Itasca Consulting Group: Minneapolis, Minnesota, 2000.

[14] Catalano E., Chareyre B., Barthélémy F. Pore-scale modeling of fluid-particles interaction and emerging poromechanical effects. *Int. J. Numer. Anal. Meth. Geomech*., 38 (2014) 51–71.

[15] Papachristos E., Scholtès L., Donzé F.V., Chareyre B.. Intensity and volumetric characterizations of hydraulically driven fractures by hydro-mechanical simulations. *Int. J. Rock Mechanics & Mining Sciences*, 93 (2017) 163–178.

[16] Tomac I., Gutierrez M.. Coupled hydro-thermo-mechanical modeling of hydraulic fracturing in quasi-brittle rocks using BPM-DEM. *J. of Rock Mechanics and Geotechnical Engineering*, 9 (2017) 92-104.

[17] Caulk R., Sholtès L., Krzaczek M., Chareyre B.. A pore-scale thermo–hydro-mechanical model for particulate systems. *Comput. Methods Appl. Mech. Engrg.* 372 (2020) 113292.

[18] Krzaczek M., Kozicki J., Nitka M., Tejchman J. Simulations of hydro-fracking in rock mass at meso-scale using fully coupled DEM/CFD approach. *Acta Geotechnica* 15(2) (2020) 297-324.

[19] Krzaczek M., Nitka M., Tejchman J. Effect of gas content in macro-pores on hydraulic fracturing in rocks using a fully coupled DEM/CFD approach, *Int. J. Numerical and Analytical Methods in Geomechanics* 45(2) (2021) 234-264.

[20] Peng D.Y. and Robinson D.B. A new two-constant equation of state. Industrial & Engineering Chemistry Fundamentals, 15 (1976) 59–64.

[21] Kozicki J., Donzé F.V. A new open-source software developer for numerical simulations using discrete modeling methods, *Computer Methods in Applied Mechanics and Engineering* 197 (2008) 4429-4443.

[22] Šmilauer V., Chareyre B. Yade DEM Formulation, Manual, 2011.

[23] Cundall P., Hart R. Numerical modelling of discontinua, *Engineering Computations* 9 (1992) 101-113.

[24] Nitka M., Tejchman J. Modelling of concrete behaviour in uniaxial compression and tension with DEM. *Granular Matte*r 17 (1) (2015) 145-164.

[25] Widulinski L., Tejchman J., Kozicki J., Leśniewska D. Discrete simulations of shear zone patterning in sand in earth pressure problems of a retaining wall. *Int. J. Solids Struct.* 48 (7–8) (2011) 1191–1209.

[26] Kozicki J., Niedostatkiewicz M., Tejchman J., Mühlhaus H.B. Discrete modelling results of a direct shear test for granular materials versus FE results. *Granular Matter* 15 (5) (2013) 607–627.

[27] Kozicki J., Tejchman J., Műhlhaus H.B. Discrete simulations of a triaxial compression test for sand by DEM. *Int. J. Num. Anal. Meth. Geomech.* 38 (2014) 1923–1952.

[28] Kozicki J., Tejchman J. Relationship between vortex structures and shear localization in 3D granular specimens based on combined DEM and Helmholtz–Hodge decomposition. *Granular Matter* (2018) 20:48.

[29] Skarżyński L., Nitka M., Tejchman J. Modelling of concrete fracture at aggregate level using FEM and DEM based on x-ray μCT images of internal structure. *Engineering Fracture Mechanics* 10 (147) (2015) 13-35.

[30] Nitka M., Tejchman J. A three-dimensional meso scale approach to concrete fracture based on combined DEM with X-ray μCT images. *Cement and Concrete Research* 107 (2018) 11-29.

[31] Suchorzewski J., Tejchman J., Nitka M. Discrete element method simulations of fracture in concrete under uniaxial compression based on its real internal structure. *Int. J. Damage Mechanics* 27 (4) (2018) 578-607.

[32] Suchorzewski J., Tejchman J., Nitka M. Experimental and numerical investigations of concrete behaviour at meso-level during quasi-static splitting tension. *Theoretical and Applied Fracture Mechanics* 96 (2018) 720-739.

[33] Suchorzewski J., Tejchman J., Nitka M., Bobinski J. Meso-scale analyses of size effect in brittle materials using DEM. *Granular Matter* 21 (9) (2019) 1-19.

[34] Nitka M., Tejchman J. Meso-mechanical modelling of damage in concrete using discrete element method with porous ITZs of defined width around aggregates. *Engineering Fracture Mechanics* 231 (2020) 107029.

[35] Reynolds O. An experimental investigation of the circumstances which determine whether the motion of water shall be direct or sinous, and of the law of resistances in parallel channels. *Phil. Trans. Roy. Soc*., London, 174 (1883) 935-982.

[36] Batchelor G. An Introduction to Fluid Dynamics, Cambridge University Press, Cambridge, 2000.

[37] Barmak I., Gelfgat A., Vitoshkin H., Ullmann A., Brauner N. Stability of stratified two-phase flows in horizontal channels. *AIP Physics of Fluids* 28 (2016), doi: 10.1063/1.4944588.

[38] Mathias P.M., Naheiri M., Oh E.M. A Density Correction for the Peng-Robinson Equation of State. Elsevier Science Publishers B.V., Amsterdam, Fluid Phase Equilibria, 47 (1989) 77-87.

[39] Peneloux A., Rauzy E.R., Freze. A Consistent Correction for Redlich-Kwong-Soave Volumes. *Fluid Phase Equilibria*, 8 (1982), 7-23.